ACS Combinatorial Science

Research Article

pubs.acs.org/acscombsci

Combinatorial Discovery of Cosolvent Systems for Production of Narrow Dispersion Thiolate-Protected Gold Nanoparticles

O. Andrea Wong, W. Scott Compel, and Christopher J. Ackerson*

Department of Chemistry, Colorado State University, Fort Collins, Colorado 80523, United States

Supporting Information

ABSTRACT: The effect of aqueous solvent concentration in the synthesis of water-soluble thiolate-protected gold nanoparticles (AuNPs) was investigated for 13 water-miscible solvents and three thiolate ligands (*p*-mercaptobenzoic acid, thiomalic acid, and glutathione). The results were analyzed by construction of heat maps that rank each reaction result for polydispersity. When solvents were organized in the heat map according to their Dimroth–Reichardt E_T parameter (an approximate measure of polarity), two "hot spots" become apparent that are independent of the ligand used. We speculate that one hot spot may arise in part from the metal chelation or coordination ability of solvents that include diglyme, 1,2-dimethoxyethane, 1,4-dioxane, and tetrahydrofuran. The second hot spot arises at concentrations of alcohols including 2-propanol and 1-butanol that appear to selectively precipitate a growing product, presumably stopping its growth at a certain size. We observe some tightly dispersed products that appear novel. Overall, this study expands the number of tightly dispersed water-soluble AuNPs that can be directly synthesized.

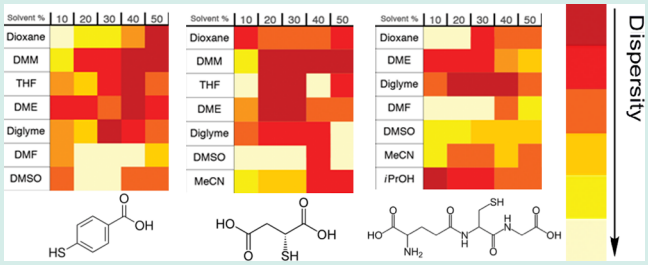

KEYWORDS: *thiolate-protected gold nanoparticles, solvent screen, p-mercaptobenzoic acid, thiomalic acid, glutathione*

INTRODUCTION

The landmark Brust–Schiffrin synthesis[1,2] and its derivatives[3−6] preceded a now large body of literature concerning thiolate-ligated gold nanoparticles (AuNPs). This synthesis generally produces polydisperse products which can be purified,[7] etched,[7,8] annealed or "size-focused"[9,10] to give products of atomically precise formulas.[11,12] The 5, 8, 14, 21, and 29 kDa products identified earlier[13−16] are now assigned as $Au_{25}(SR)_{18}$, $Au_{36}(SR)_{24}$, $Au_{38}(SR)_{24}$, $Au_{40}(SR)_{24}$, $Au_{67}(SR)_{35}$, $Au_{102}(SR)_{44}$, and $Au_{144}(SR)_{60}$.[17−22] The special stabilities of these clusters are explained by electronic or geometric shell filling.[23,24] The widespread adoption of these compounds by chemists,[25] biologists,[26] and physicists[27] is a testament to their robust nature.

Methods based on oxidative etching are now widespread for synthesis of the especially stable clusters.[10,28−31] These methods excel at isolating exceptionally stable clusters with nonpolar ligand shells. Also, the purification of well-defined nanoclusters from similarly sized clusters, such as the purification of $Au_{38}(SR)_{24}$ from $Au_{40}(SR)_{24}$, is increasingly well developed.[32,33] For water-soluble clusters (needed for biological applications), application of etching methods is much more limited, and is shown only for two cases so far.[34,35] Synthetic methods are also lagging for clusters that are insufficiently stable to survive the etching process.[21,36]

A less mature method for limiting the polydispersity of a cluster preparation involves selection of reaction conditions so that a single nanocluster product, rather than a product distribution, is favored. This method was developed for water-soluble clusters, notably the *p*-mercaptobenzoic acid (*p*MBA) protected $Au_{144}(pMBA)_{60}$ and $Au_{102}(pMBA)_{44}$ clusters.[36,37] Reaction conditions that produced these syntheses were found by screening each of the synthetic parameters in the Brust synthesis, including ligand:Au ratio, solvent composition, and reductant molar excess. The direct synthesis differs from etching methods in that ligand is generally not present in excess. Compared to the now relatively mature etching approaches, this direct-synthesis approach may allow production of "less stable" clusters, presently synthetically elusive clusters,[3,5,6] and a larger panel of biologically useful water-soluble clusters than is presently available.

Previous work speculated that solvent composition is among the most important parameters in this direct synthesis of nanoparticles.[7,37] Herein we attempt to gain additional insight into which solvent compositions are associated with narrow dispersion in the Brust-type synthesis. By screening in a combinatorial manner the synthetic effects of aqueous compositions of 13 water-miscible solvents, we observe the emergence of hot spots of overall solvent polarity associated with very narrow product distribution. Overall our results suggest the existence of several so far unidentified discrete water-soluble nanoparticles.

Received: May 1, 2014
Revised: November 18, 2014
Published: December 2, 2014

 © 2014 American Chemical Society

RESULTS

Previous work suggests that two of the most important parameters for direct synthesis are ligand identity and solvent composition. We reasoned that systematic investigation of these two synthetic influences may reveal promising synthetic conditions for novel products. We tested the ligands *p*-mercaptobenzoic acid (*p*MBA), thiomalic acid (Tm), and glutathione (GSH, deprotonated: GS) in systematically varied aqueous mixtures of the solvents 1,4-dioxane (dioxane), dimethoxymethane (DMM), tetrahydrofuran (THF), dimethoxyethane (DME), diethylene glycol dimethyl ether (diglyme), *N*,*N*-dimethylformamide (DMF), dimethyl sulfoxide (DMSO), acetonitrile (MeCN), 2-propanol (*i*PrOH), 1-butanol (*n*BuOH), 1-propanol (*n*PrOH), ethanol (EtOH), and methanol (MeOH).

The general approach to the combinatorial screening of reaction conditions involved attempting as many as 96 reactions, examining the effect of two synthetic variables at a time, in a matrix as large as 12 × 8. Each reaction was analyzed initially by polyacrylamide gel electrophoresis[7,8] (PAGE). To enable facile comparison of reaction conditions, we scored each lane of analytical PAGE gel corresponding to each tested reaction condition. The scoring system extracts three key pieces of information on a direct synthesis condition: (1) how many products were produced; (2) the apparent dispersity of the products; (3) the relative sizes of the products. An example of how we scored a small set of reactions run in varying concentrations of aqueous ethanol is shown in Figure 1.

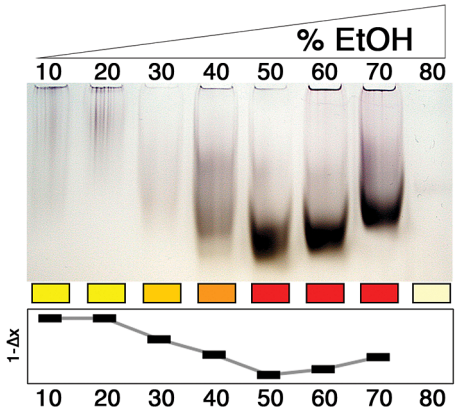

Figure 1. Example of a scored PAGE gel, showing heat map that encodes dispersity, and a relative size graph. The darker red in the heat map indicates a more tightly dispersed product and the relative size graph on the bottom encodes the mobility (i.e., relative size) of the products within the same gel.

Relative dispersity is shown as a heat value and relative size and number of products are depicted in the bottom panel. Overall, this scoring system allows compact comparison of the effects of solvent system and ligand choice in gold nanoparticle synthesis. While the PAGE gels give an excellent comparison of synthetic conditions, they may not fully account for minor products present.

Solvent Effects on Synthesis of *p*-Mercaptobenzoic Acid (pMBA) Protected Clusters. The solvent screen with *p*MBA was carried out with a 1:3.4 Au/*p*MBA ratio with initial [Au] = 2 mM and 1 equiv of $NaBH_4$ with respect to Au. These initial screening parameters are similar to those of the published $Au_{102}(pMBA)_{44}$ synthesis which serve as a good starting point for our initial screen.[16,31] The reactions were allowed to proceed for 17 h at 30 °C in a shaking incubator. All reactions were identical except for the solvent composition. We attempted synthesis in aqueous mixtures of each of the 13 solvents, with solvent compositions ranging from 10% to 80% solvent in water. The results of this solvent screen are shown in Figure 2.

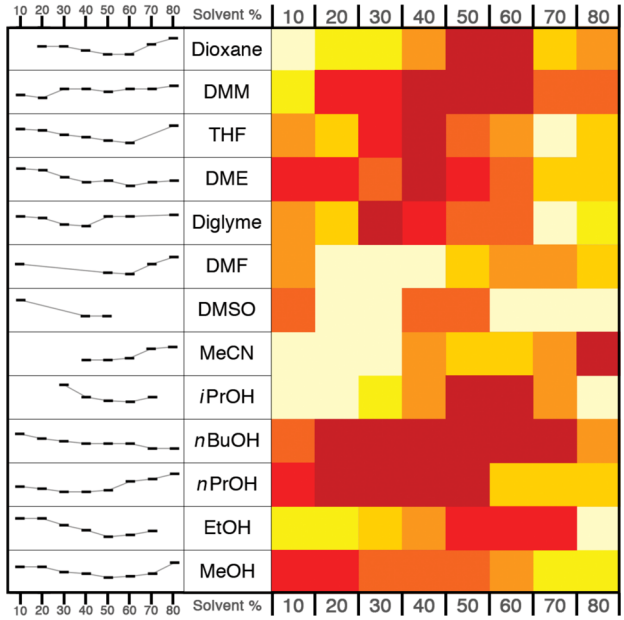

Figure 2. Solvent screen results for the synthesis of gold nanoparticles using *p*MBA as the ligand. Left panel shows the relative size of the clusters as shown by PAGE analysis. The conditions that lack a size indicator indicate no visible product formation. The right panel shows the dispersity of the products with the darkest red being the most monodispersed product. The pale yellow squares indicate no visible product formation.

Figure 2 shows the relative size of the product (with the *y*-axis defined as 1 − Δ*x* to resemble the bands on the original polyacrylamide gel, Δ*x* is the distance the product traveled from the well). Some screened conditions yield either no product or nonvisible product and those conditions do not have a marker on the relative size graph and these are displayed as pale yellow space in the heat map. The Δ*x* for the polydispersed products is measured in the center of the product streak.

The right panel of Figure 2 shows the dispersity of the product, with tighter dispersion indicated by darker red, and wider dispersion indicated by lighter colors. The *x*-axis of Figure 2 is organized according to the percentage cosolvent in water. We constructed preliminary heat maps with the solvent identity (*y*-axis) arranged according to dielectric constant, dipole moment, chelating ability, and density (Supporting Information Figures S1−S12) and observed that when solvents are organized according to polarity (or ionizing power, Dimroth−Reichardt E_T parameter[9,10]) of the solvents, hot spots become apparent that are independent of ligand used. We discounted the possibility that the redox potential of the solvents may play a role in product formation because the Au is in redox-stable −Au(I)−SR− complexes before it is exposed to solvents other than water, and we do not see evidence for

oxidation or reduction upon solvent addition as judged by stable color of the solutions that form.

Table 1 gives a listing of E_T parameters for each solvent used. Figure 2 and other heat maps shown in this paper arrange the solvents from least-polar to most polar. The value of E_T parameter of DMM was not available. For the purpose of the heat maps, DMM was placed between dioxane and THF using the dielectric constant of the three solvents.

Table 1. Solvent Used in the Synthetic Screening As Ranked in Dimroth−Reichardt E_T parameter[35]

solvent	Dimroth−Reichardt E_T parameter (kcal/mol)
1,4-dioxane	36.0
dimethoxymethane (DMM)	N/A
tetrahydrofuran (THF)	37.4
1,2-dimethoxyethane (DME)	38.2
diethylene glycol dimethyl ether (diglyme)	38.6
dimethylformamide (DMF)	43.8
dimethyl sulfoxide (DMSO)	45.1
acetonitrile (MeCN)	45.6
2-propanol (*i* PrOH)	49.2
1-butanol (*n* BuOH)	50.2
1-propanol (*n* PrOH)	50.7
ethanol (EtOH)	51.9
methanol (MeOH)	55.4

In Figure 2 there are two hot spots, one centered at 50% DMM and another centered at 40% *n*BuOH. On the basis of 1 − Δx values, the products created at these hot spots are not identical. Because of similarities between the hot spots found in the *p*MBA screen and those found for other ligands, we present a unified, expanded discussion below.

Using $Au_{102}(pMBA)_{44}$ and $Au_{144}(pMBA)_{60}$ as standard markers in each PAGE analysis, we found eight solvent conditions that make monodispersed products, as judged by the appearance of a single, very discrete band in PAGE. Some of these solvent conditions yield products that are in between $Au_{102}(pMBA)_{44}$ and $Au_{144}(pMBA)_{60}$. These conditions include (50−60% *i*PrOH, 40% THF, 50−60% dioxane, 30% diglyme, and 40% DME). As judged by relative gel mobility, it is likely that one or more of these products is novel, and not, for instance Au_{130}.[36]

Other conditions are notable for making particles larger than $Au_{144}(SR)_{60}$, including 20−70% *n*BuOH, 80% MeCN, and 40−60% DMM. The conditions that makes that most monodispersed products are correlated to the darkest red spots in the heat map.

We further characterized the products of some of the reactions that produced narrow dispersity products by transmission electron microscopy. Figure 3 shows transmission electron micrographs for the 40% THF and 60% *n*BuOH conditions corresponding to products from each hotspot in Figure 2. TEM reveals narrow dispersity products in each case, with the 40% THF condition corresponding to 1.84 nm ±0.30 nm nanoparticles and the 60% nBuOH condition corresponding to 1.96 ± 0.29 nm. The approximate diameters correspond to molecular formulas of $Au_{228}pMBA_{75}$ and $Au_{188}pMBA_{66}$, respectively. Some of the apparent dispersity in this measurement may be attributed to the difficulty in determining the precise edge of sub-5-nm diameter particles in transmission electron micrographs—most of the measured dispersity may be inherent to the TEM technique itself as applied here. Some of the dispersity, especially larger particles, may also be attributed to electron-beam induced sintering of adjacent particles. The particles appear spherical in morphology in each case, and are of sufficiently tight dispersity to form extended 2D hexagonal lattices.

After identifying the hotspots, we sought to improve the existing direct synthesis for $Au_{102}(pMBA)_{44}$. The existing literature synthesis uses 47% aq. MeOH, [Au] = 3 mM,

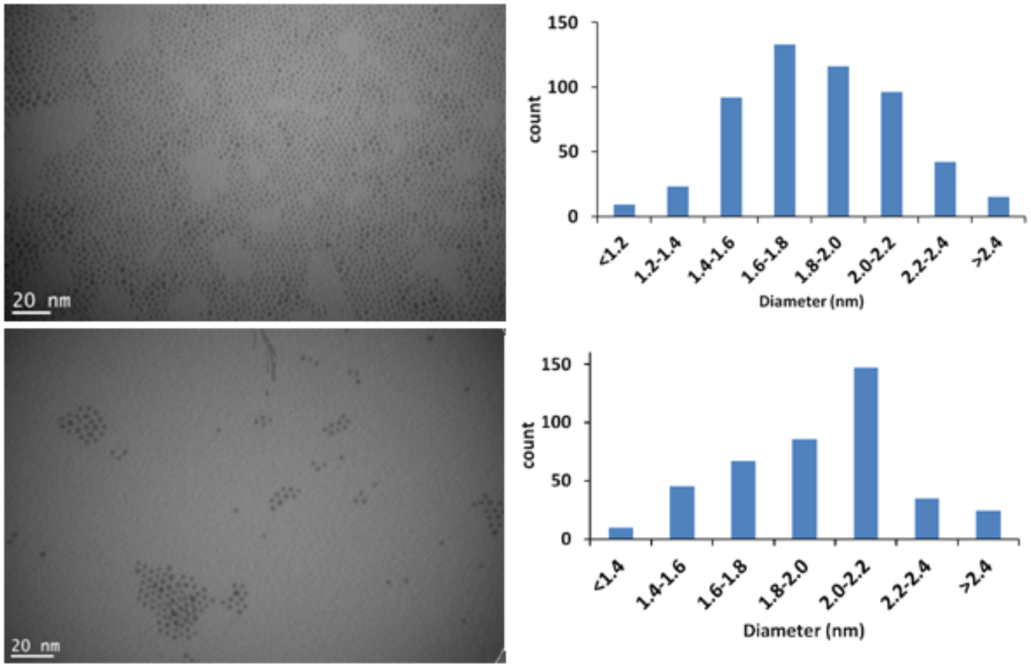

Figure 3. TEM image and histogram of the *p*MBA-protected gold nanoclusters synthesized using 40% THF (top, 1.84 ± 0.30 nm, $Au_{188}pMBA_{66}$) and 60% *n*BuOH (bottom, 1.96 ± 0.29 nm, $Au_{228}pMBA_{75}$).

dx.doi.org/10.1021/co500072c | ACS Comb. Sci. 2015, 17, 11−18

[*p*MBA] = 12 mM, at a 0.036 mmol Au scale. Four solvent conditions emerged to make clusters that have the same $1 - \Delta x$ values on the PAGE analysis (80% *n*BuOH, 10% DMF, 10% diglyme, and 50% MeOH). A series of refinements, including the adjustment of solvent percentages in finer increments, order of addition, method of addition, temperature, [*p*MBA], [BH_4^-], degassed solvents vs nondegassed solvents, equilibration time of the polymer, and the addition of solid $NaBH_4$ vs aqueous $NaBH_4$ were carried out for the synthesis of $Au_{102}(pMBA)_{44}$. We came to a condition that allows us to make $Au_{102}pMBA_{44}$ in a 0.5 mmol Au scale in reasonable purity and yield. The reaction is 50 times larger than the original reactions scale and reproducibility may be improved. The synthetic condition changes to the published synthesis are minor, suggesting that the published synthesis was already very well optimized. We found that the published solvent (47% aq. MeOH) made the most monodispersed $Au_{102}(pMBA)_{44}$. Operational changes that improved the reproducibility and scalability include the rapid mixing of the reagents during polymer synthesis and using solid $NaBH_4$ instead of an aqueous solution. Notably, the approach does not allow elimination of the second product almost always observed in $Au_{102}(pMBA)_{44}$ syntheses that is generally removed by fractional precipitation.

Solvent Effects on Synthesis of Thiomalate (Tm) Protected Clusters. Similar to the initial solvent screen with *p*MBA, the solvent screen with Tm as the ligand was carried out with 1:3 Au/Tm ratio with [Au] = 2 mM and 1.5 equiv of $NaBH_4$ with respect to Au. The reactions were allowed to proceed for 17 h at 30 °C in a shaking incubator. The results of this solvent screen are shown in Figure 3.

A hotspot appears centered at 30% THF, with additional areas of tight dispersity observed in isolated conditions of 60 and 80% *n*BuOH, and 10% and 60−70% EtOH (shown as dark red squares in the heat map). Thus, the optimal solvent for synthesis of narrowly dispersed products using Tm as the ligand can be found in the low percentages of the lower polarity solvents, except in the case of *n*BuOH which appears to be advantageous to monodispersity at all percentages. The large hot spot at lower concentrations of solvent may share a phenomenological origin with the similar hotspot for *p*MBA, with a shift toward lower cosolvent concentrations arising because Tm is more charged (thus more polar) compared to *p*MBA.

Many of the solvents result in two distinguishable tight bands (dioxane, DME, MeCN, *n*PrOH, and EtOH), as shown in the depiction of two products in the left panel. Since the heat map considers the entire reaction, some of these conditions are scored as polydisperse, even though they may contain notably monodisperse individual products.

The smaller band in each of the two product producing reactions can be further resolved into three products, notable for their distinctive colors (red, green, and yellow; Figure 4, left). These are similar to the colors reported by Tsukuda,[37] for GSH protected clusters smaller than $Au_{25}(SG)_{18}$. The color order does not match, however, so suggestions of molecular formula cannot be made by analogy, other than these are likely to be clusters smaller than $Au_{25}(SR)_{18}$.

To demonstrate the potential of systematic screening of reaction conditions, we further refined the synthesis that produces this set of three products, so that that only the red product is produced (Figure 4, right). The refinement process included adjustment of temperature, Au:Tm ratio, pH, reaction time, [NaOH], amount of O_2 in the solvent, and [BH_4^-] (see

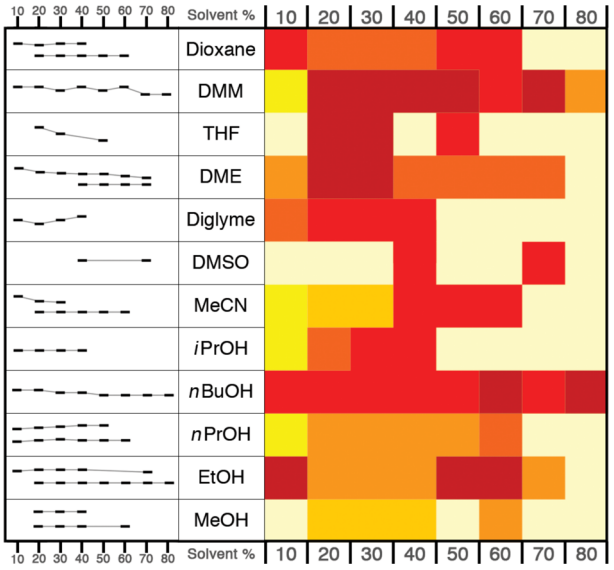

Figure 4. Solvent screen results for the synthesis of gold nanoclusters using Tm as the ligand. The left panel shows the relative size of the clusters as shown by PAGE analysis. The conditions that lack a size marker indicate no visible product formation. The conditions that have two size markers indicate the formation of two relatively tight bands. The right panel shows the dispersity of the products with the darkest red being the most monodispersed product. The pale yellow squares indicate no visible product formation.

Experimental Procedures for the synthesis of the red product). The parameters that have been adjusted are commonly screened parameters in the refinement of gold nanocluster syntheses in our laboratory. The refinement process is mainly determined by the results of the previous screen until no further optimization can be obtained. Some parameters, such as [$NaBH_4$], need to be revisited after other parameters are set.

Solvent Effects on Synthesis of Glutathione (GSH) Protected Clusters. The solvent screen with GSH as the ligand was carried out with 1:3 Au/GSH with [Au] = 2 mM and 3 equiv of BH_4^- with respect to Au. The reactions were allowed to proceed for 2 h and 15 min at 4 °C. These conditions were the result of an initial optimization. The result of this solvent screen is shown in Figure 5. As in the case for

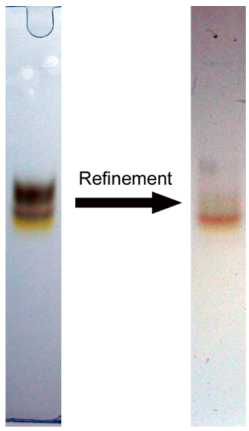

Figure 5. Refinement progress of the "triple product" band to a red band. The PAGE lane on the left is the "triple product" band before the refinement process and the PAGE lane on the right is the resulting red band after the refinement process.

dx.doi.org/10.1021/co500072c | *ACS Comb. Sci.* 2015, 17, 11−18

other ligands, we observe two hot spots in the heat map. One can be found in the low to mid percentages (20−40%) of low polarity solvents (DME and diglyme), the second is found in the low percentages (10−30%) of the alcohols (*i*PrOH, *n*BuOH, and *n*PrOH).

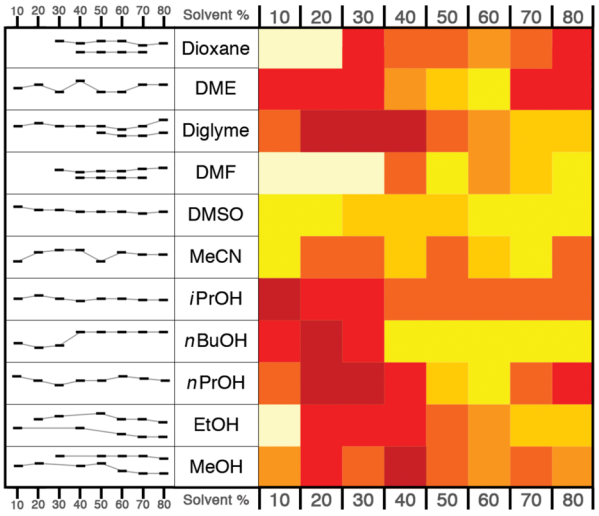

Figure 6. Solvent screen results for the synthesis of gold nanoclusters using GSH as the ligand. Left panel shows the relative size of the clusters as shown by PAGE analysis. The conditions that lack a size indicator indicate no visible product formation. The conditions that have two size markers indicate the formation of two relatively tight bands. The right panel shows the dispersity of the products with the darkest red being the most monodispersed product. The pale yellow squares indicate no visible product formation.

The products observed at the hot-spots when GSH is used as a ligand are less than 1.5 nm in diameter and essentially of insufficient size for routine and accurate analysis by transmission electron microscopy. To characterize the approximate composition and dispersity of GSH protected nanoparticles we used size exclusion chromatography. A Superdex 75 gel filtration column (GE Health Sciences) is used routinely to separate proteins in the 3 to 70 kDa range. By comparison of actual and computed Stokes−Einstein radii, we estimate that the column is capable of resolving spherical clusters with approximate formulas of $Au_{10}(SG)_{11}$ to $Au_{998}(SG)_{161}$. We calibrated with protein standards as described in the methods section and shown in Supporting Information Figure S18. We tested experimentally the elution of the product synthesized at 76% aqueous diglyme, which appears to contain several products as observed in the PAGE, although one product appears more abundant (Supporting Information Figure S16). By chromatographic analysis we see that the 76% diglyme product also contains many products and similar to the appearance in the gel, a single product dominates. The dominant product has a Stokes−Einstein radius of 1.11 nm (Figure 7), corresponding to an approximate molecular formula of $Au_{53}(GS)_{26}$. To arrive at this approximate molecular formula, we assume that GSH contributes 0.35 nm to the total hydrodynamic diameter of 2.44 nm, as calculated previously.[11] The remaining diameter is occupied by gold atoms. The full-width at half-maximum of the main peak is slightly broader than that of the protein standards injected, consistent with a the appearance of the second most abundant product in the gel at lower molecular weight, and the tailing at what corresponds to

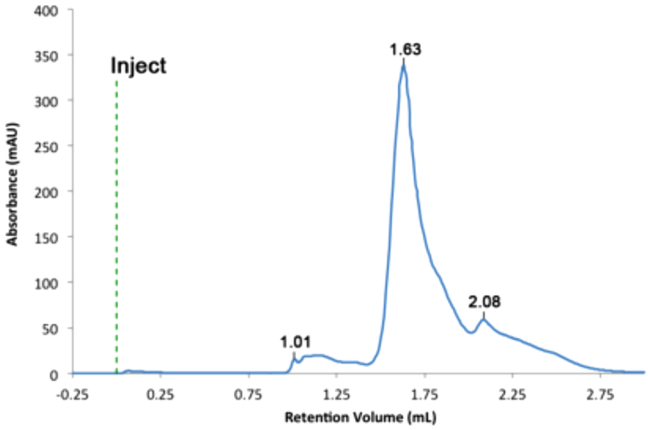

Figure 7. Superdex 75 Elution Profile for GS protected nanoparticles synthesized in 76% diglyme.

lower molecular weight also suggests that the PAGE gel is an accurate depiction of the dispersity of the sample.

One goal at the outset of this screen was to attempt to find a direct, large scale synthesis of $Au_{25}(GS)_{18}$.[7,35,38] We found that one of our screened solvent conditions produced a product with the expected orange appearance, and approximately expected gel mobility. MALDI characterization of this product is not consistent with $Au_{25}(GS)_{18}$ and is instead consistent with a novel nanocluster with properties that are the subject of a future report. It is presently unclear if it is possible to directly synthesize $Au_{25}(GS)_{18}$ with this direct synthesis approach.

DISCUSSION

Two hot spots of high monodispersity appear in each of the combinatorial solvent screens, independent of the organothiolate ligand that protects the resulting nanoparticles. One of the hot spots occurs in lower polarity solvents such as dioxane, DME, THF, and diglyme. These solvents are interesting in that, with the exception of THF, each is potentially both a solvent and a metal chelating ligand (Figure 6). These coordinating or chelating solvents may interact with either the $(Au\text{-}SR)_n$ polymer precursors, perhaps to enforce a particular polymer size prior to the $NaBH_4$ reduction step. This is suggested by others as a means to narrow the dispersity of cluster syntheses.[39] These solvents may also interact competitively with organothiolates to occupy the Au^0 surfaces of nanoclusters. The multidentate nature of these ligands and their extraordinarily high concentration relative to thiols may make these oxygen-containing molecules capable of such competition. We speculate that either one of these effects may help to stabilize a particular cluster molecular formula, leading to the observed narrow dispersity.

The other hot spot appears for alcohols with longer hydrophobic chains, such as *i*PrOH, *n*BuOH, and *n*PrOH. We speculate that this hot spot arises because the nanoclusters grow until they reach a size at become insoluble in the aqueous alcohol mixture, at which point they precipitate. The precipitated nanoclusters then cease to grow. Under these circumstances, growing and completed clusters are separated in two physical phases, resulting in narrow size distribution.

This work highlights several solvents that do not correlate with monodisperse product preparation. Solvents that do not appear to produce narrow dispersion products include MeOH DMF, DMSO, and MeCN. The absence of monodisperse products in methanol is of special note. Most water-soluble

thiolate ligated gold nanoclusters reported to date are synthesized in aqueous methanol.[7,35−38,40−43] We observe here that methanol consistently results in more polydispersed product than its more nonpolar and more bulky counterparts.

CONCLUSIONS

Early work on thiolate protected gold nanoclusters identified the approximate masses of especially abundant (magic-sized) clusters. Etching or size-focusing methods now reliably produce these clusters in many laboratories around the world with organic ligand shells. Synthetic methods for making water-soluble clusters and also particles that do not conform to the "magic" sizes are not yet widely available. By combinatorial screening of solvent conditions we observe hot spots of low product dispersity, suggesting routes for direct synthesis of well-defined water-soluble particles. We also observe in some cases the synthesis of well-defined products of sizes apparently in between the magic sizes. For instance we observe five solvent conditions that produce narrow dispersity products that are between $Au_{102}(p\text{MBA})_{44}$ and $Au_{144}(p\text{MBA})_{60}$. From the combinatorial solvent screen, there seem to be two modes of solvent effects: chelating or coordinating ability of the solvent and cluster solubility in the solvent. Full development of either one of these modes may greatly expand the availability of water-soluble clusters for applications in biology, for instance as contrast markers,[44] delivery vectors,[4] or RF heating antennae.[45]

EXPERIMENTAL PROCEDURES

Materials. All commercially available reagents were used without further purification. Tetrachloroauric (III) acid ($HAuCl_4{\cdot}3H_2O$ 99.99% metal basis, Alfa Aesar), *p*-mercaptobenzoic acid (>95.0%, TCI America), L-glutathione reduced (≥98%, Sigma-Aldrich), thiomalic acid (≥99.0%, Sigma-Aldrich), $NaBH_4$ (98−99%, MP Biomedicals), 1,4-dioxane (ACS grade, Mallinckrodt Chemicals), tetrahydrofuran (ACS grade, Mallinckrodt Chemicals), dimethoxyethane (99+%, Alfa Aesar), diethylene glycol dimethyl ether (99%, Sigma-Aldrich), dimethylformamide (reagent grade, Amresco), dimethyl sulfoxide (99.9% Fisher Scientific), acetonitrile (ACS grade, Fisher Scientific), 2-propanol (ACS grade, Fisher Scientific), 1-butanol (ACS grade, Fisher Scientific), 1-propanol (99.0%, Mallinckrodt Chemicals), ethanol (200 proof ACS grade, Pharmco-AAPER), methanol (99.9%, Fisher Scientific), and dimethoxymethane (98%, Alfa Aesar). Nanopure water (resistivity 18.2 MΩ-cm) was produced with a Barnstead NANOpure water system.

Solvent Screen Procedures. *Solvent Screen with p-Mercaptobenzoic Acid as the Ligand. Synthesis of Polymer with p-Mercaptobenzoic Acid:* *p*-Mercaptobenzoic acid (3.4 mmol, 0.524 g, 3.4 equiv) was dissolved in H_2O (24 mL), and 10 M aq. NaOH (1.6 mL) was added to the suspension. The resulting solution was mixed; the pH was determined to be >13, and the solution was diluted with H_2O to a final volume of 50 mL. $HAuCl_4{\cdot}3H_2O$ (1 mmol, 0.394 g, 1 equiv) was dissolved in H_2O (50 mL) in a separate beaker. The *p*MBA solution and the gold solution were mixed to yield a clear bright red solution. The bright red solution was stirred at rt overnight, which changes to yellow after about 1 h.

96-Well Plate Solvent Screen: Fifty microliters of the above polymer solution was distributed in each well using a multichannel pipet, and the appropriate amount of organic solvent was added to each well (e.g., 25 μL for 10%, 200 μL for 80%); then, it was backfilled with the appropriate amount of H_2O (e.g., 175 μL for 10%, 0 μL for 80%) to result in a final reaction volume of 250 μL. Four microliters of freshly made 0.125 M aq. $NaBH_4$ was added to each well with a multichannel pipet. The 96-well plate was then placed in an incubating shaker at 30 °C for 17 h MeOH (1 mL) and 2.0 M NH_4OAc (25 μL) was added to each well and the 96-well plate was centrifuged in a swinging bucket rotor at 4000 rpm and 4 °C for 10 min. The clear and colorless supernatant was then removed with a multichannel pipet and the precipitate was air-dried. Gel electrophoresis visualization was run on a 15% polyacrylamide gel (19:1, acrylamide/bis(acrylamide)) at 110 V for 1.5 h. The nanoparticle bands were visible by eye and with a UV transilluminator, thus no staining steps were performed for visualization.

Solvent Screen with Thiomalic Acid as the Ligand. Synthesis of Polymer with Thiomalic Acid: Thiomalic acid (3.0 mmol, 0.450 g, 3.0 equiv) was dissolved in H_2O (20 mL), 10 M aq. NaOH (2.0 mL) was added to the suspension. The resulting solution was mixed; the pH was checked to be >13, and the solution was diluted with H_2O to a final volume of 50 mL. $HAuCl_4{\cdot}3H_2O$ (1 mmol, 0.394 g, 1 equiv) was dissolved in H_2O (50 mL) in a separate beaker. The thiomalic acid solution and the gold solution were mixed to yield a clear bright red solution. The bright red solution was stirred at rt overnight, which changes to yellow after about 1 h.

96-Well Plate Solvent Screen: Fifty microliters of the above polymer solution was distributed in each well using a multichannel pipet, and the appropriate amount of organic solvent was added to each well (e.g., 25 μL for 10%, 200 μL for 80%); then, it was backfilled with the appropriate amount of H_2O (e.g., 175 μL for 10%, 0 μL for 80%) to result in a final reaction volume of 250 μL. Three microliters of freshly made 0.25 M aq. $NaBH_4$ was added to each well with a multichannel pipet. The 96-well plate was then placed in an incubating shaker at 30 °C for 17 h. MeOH (1 mL) and 2.0 M NH_4OAc (25 μL) was added to each well and the 96-well plate was centrifuged in a swinging bucket rotor at 4000 rpm and 4 °C for 10 min. The clear and colorless supernatant was then removed with a multichannel pipet and the precipitate was air-dried. Gel electrophoresis visualization was run on a 15% polyacrylamide gel (19:1, acrylamide: bis(acrylamide)) at 110 V for 1.5 h. The nanoparticle bands were visible by eye and with a UV transilluminator, thus no staining steps were performed for visualization.

Direct Synthesis of Thiomalic Acid-Protected Red AuNP (Figure 4, Right). In a 15 mL conical tube, 1 mL of Au−Tm polymer solution (from above, 0.01 mmol Au), 2.5 mL of DME, and 1.5 mL of H_2O were added in order. The reaction was allowed to cool in a 4 °C fridge for 10 min; 60 μL of 0.25 M $NaBH_4$ (0.015 mmol, 1.5 equiv. with respect to Au) was added, and the reaction was gently mixed and left to sit at 4 °C (without mixing/shaking) for 3 days. MeOH was then added to the reaction to a total volume of 15 mL; 200 μL of 2.0 M NH_4OAc was also added, and the reaction was then shaken to mix and was centrifuged at 4 °C for 10 min. The supernatant was removed, and the resulting pellet (red product) was air-dried. Gel electrophoresis visualization was run on a 22% polyacrylamide gel (19:1, acrylamide: bis(acrylamide)) at 110 V for 1.5 h. The nanoparticle bands were visible by eye and with a UV transilluminator, thus no staining steps were performed for visualization.

Solvent Screen with Glutathione as the Ligand. 96-Well Plate Solvent Screen with L-Glutathione as the Ligand: $HAuCl_4 \cdot 3H_2O$ (111.2 mg) was dissolved in H_2O (2.824 mL) in a 15 mL conical tube to yield a 100 mM Au solution. L-Glutathione (169.4 mg) was dissolved in 0.3 M aq. NaOH (5.512 mL) in a separate conical to yield a 100 mM glutathione solution (pH = 9.5). Ten microliters of Au solution and then 30 μL of glutathione solution were added to each well of a 96-well plate. The appropriate amount of H_2O (e.g., 400 μL for 10% and 50 μL for 80%) and then the appropriate amount of organic solvent (e.g., 50 μL for 10% and 400 μL for 80%) were added. The resulting solution was shaken at 4 °C for 45 min. Ten microliters of freshly made 300 mM aq. $NaBH_4$ was added to each well (500 μL total reaction volume), and the plate was shaken at 4 °C for 2 h and 15 min. MeOH (1 mL) and 2.0 M NH_4OAc (25 μL) was added to each well and the 96-well plate was centrifuged in a swinging bucket rotor at 4000 rpm and 4 °C for 10 min. The supernatant was then removed with a glass pipet connected to an aspirator, and the precipitate was dried under vacuum overnight. Gel electrophoresis visualization was run on a 22% polyacrylamide gel (19:1, acrylamide: bis-(acrylamide)) at 110 V for 1.5 h. The nanoparticle bands were visible by eye and with a UV transilluminator; thus, no staining steps were performed for visualization.

Transmission Electron Microscopy. Imaging was performed with a JEOL 1400 at an acceleration voltage of 100 kV and images were recordeed on Orius SC1000 (~4kx3k). The gold nanocluster samples were applied to carbon support film on 400 mesh copper speciment grids. The excess liquid was blotted with a piece of filter paper, and the grids were allowed to dry in air.

Size Exclusion Chromatography. Separation of cluster compounds were conducted on an ÄKTApurifier HPLC system equipped with a Superdex 75 PC 3.2/30 (2.4 mL) size exclusion column. Detection was performed at a wavelength of 254 nm. Samples were injected in Nanopure H2O and eluted at 0.02 mL/min in phosphate buffer (50 mM sodium phosphate, 150 mM NaCl, pH 7.0). Thyroglobulin, γ-globulin, ovalbumin, myoglobin, aprotinin, and vitamin B-12 correesponding to Stokes–Einstein radii of 8.6, 5.1, 2.8. 1.9, 1.35, and 0.85 nm were used to generate a calibration curve for the column.

■ ASSOCIATED CONTENT

Ⓢ Supporting Information

Table of solvent properties, heat maps of the solvent screens arranged according to different solvent properties, and additional information on the thiomalic acid solvent screen. This material is available free of charge via the Internet at http://pubs.acs.org.

■ AUTHOR INFORMATION

Corresponding Author

*E-mail: ackerson@mail.colostate.edu.

Notes

The authors declare no competing financial interest.

■ ACKNOWLEDGMENTS

This work was supported by Colorado State University. The work was completed while C.J.A. was an American Federation for Aging Research New Investigator.

■ REFERENCES

(1) Brust, M.; Walker, M.; Bethell, D.; Schiffrin, D.; Whyman, R. Synthesis of thiol-derivatized gold nanoparticles in a two-phase liquid–liquid system. *J. Chem. Soc., Chem. Commun.* **1994**, 801–802.

(2) Brust, M.; Fink, J.; Bethell, D.; Schiffrin, D.; Kiely, C. Synthesis and reactions of functionalized gold nanoparticles. *J. Chem. Soc., Chem. Commun.* **1995**, 1655–1656.

(3) Dass, A. Mass spectrometric identification of $Au_{68}(SR)_{34}$ molecular gold nanoclusters with 34-electron shell closing. *J. Am. Chem. Soc.* **2009**, *131*, 11666–11667.

(4) Bowman, M.-C.; Ballard, T. E.; Ackerson, C. J.; Feldheim, D. L.; Margolis, D. M.; Melander, C. Inhibition of HIV fusion with multivalent gold nanoparticles. *J. Am. Chem. Soc.* **2008**, *130*, 6896–6897.

(5) Templeton, A.; Wuelfing, W.; Murray, R. Monolayer-protected cluster molecules. *Acc. Chem. Res.* **2000**, *33*, 27–36.

(6) Wyrwas, R. B.; Alvarez, M. M.; Khoury, J. T.; Price, R. C.; Schaaff, T. G.; Whetten, R. L. The colours of nanometric gold—Optical response functions of selected gold-cluster thiolates. *Eur. Phys. J. D* **2007**, *43*, 91–95.

(7) Schaaff, T.; Knight, G.; Shafigullin, M.; Borkman, R.; Whetten, R. Isolation and selected properties of a 10.4 kDa gold:glutathione cluster compound. *J. Phys. Chem. B* **1998**, *102*, 10643–10646.

(8) Schaaff, T.; Whetten, R. Controlled etching of Au:SR cluster compounds. *J. Phys. Chem. B* **1999**, *103*, 9394–9396.

(9) Reichardt, C. Solvatochromic dyes as solvent polarity indicators. *Chem. Rev.* **1994**, *94*, 2319–2358.

(10) Qian, H.; Zhu, Y.; Jin, R. Size-focusing synthesis, optical and electrochemical properties of monodisperse $Au_{38}(SC_2H_4Ph)_{24}$ nanoclusters. *ACS Nano* **2009**, *3*, 3795–3803.

(11) Wong, O. A.; Hansen, R. J.; Ni, T. W.; Heinecke, C. L.; Compel, W. S.; Gustafson, D. L.; Ackerson, C. J. Structure–activity relationships for biodistribution, pharmacokinetics, and excretion of atomically precise nanoclusters in a murine model. *Nanoscale* **2013**, *5*, 10525–10533.

(12) Jin, R. Quantum sized, thiolate-protected gold nanoclusters. *Nanoscale* **2010**, *2*, 343–362.

(13) Alvarez, M. M.; Khoury, J. T.; Schaaff, T. G.; Shafigullin, M.; Vezmar, I.; Whetten, R. L. Critical sizes in the growth of Au clusters. *Chem. Phys. Lett.* **1997**, *266*, 91–98.

(14) Cleveland, C. L.; Landman, U.; Schaaff, T. G.; Shafigullin, M. N.; Stephens, P. W.; Whetten, R. L. Structural evolution of smaller gold nanocrystals: The truncated decahedral motif. *Phys. Rev. Lett.* **1997**, *79*, 1873–1876.

(15) Cleveland, C. L.; Landman, U.; Shafigullin, M. N.; Stephens, P. W.; Whetten, R. L. Structural evolution of larger gold clusters. *Z. Phys. D* **1997**, *40*, 503–508.

(16) Whetten, R. L.; Khoury, J. T.; Alvarez, M. M.; Murthy, S.; Vezmar, I.; Wang, Z. L.; Stephens, P. W.; Cleaveland, C. L.; Luedtke, W. D.; Landman, U. Nanocrystal gold molecules. *Adv. Mater.* **1996**, *8*, 428–433.

(17) Heaven, M. W.; Dass, A.; White, P. S.; Holt, K. M.; Murray, R. W. Crystal structure of the gold nanoparticle $[N(C_8H_{17})_4][Au_{25}(SCH_2CH_2Ph)_{18}]$. *J. Am. Chem. Soc.* **2008**, *130*, 3754–3755.

(18) Zhu, M.; Aikens, C. M.; Hollander, F. J.; Schatz, G. C.; Jin, R. Correlating the crystal structure of a thiol-protected Au_{25} cluster and optical properties. *J. Am. Chem. Soc.* **2008**, *130*, 5883–5885.

(19) Qian, H.; Eckenhoff, W. T.; Zhu, Y.; Pintauer, T.; Jin, R. Total structure determination of thiolate-protected Au_{38} nanoparticles. *J. Am. Chem. Soc.* **2010**, *132*, 8280–8281.

(20) Nimmala, P. R.; Yoon, B.; Whetten, R. L.; Landman, U.; Dass, A. $Au_{67}(SR)_{35}$ nanomolecules: characteristic size-specific optical, electrochemical, structural properties and first-principles theoretical analysis. *J. Phys. Chem. A* **2013**, *117*, 504–517.

(21) Jadzinsky, P. D.; Calero, G.; Ackerson, C. J.; Bushnell, D. A.; Kornberg, R. D. Structure of a thiol monolayer-protected gold nanoparticle at 1.1 A resolution. *Science* **2007**, *318*, 430–433.

(22) Chaki, N. K.; Negishi, Y.; Tsunoyama, H.; Shichibu, Y.; Tsukuda, T. Ubiquitous 8 and 29 kDa gold:alkanethiolate cluster

compounds: mass-spectrometric determination of molecular formulas and structural implications. *J. Am. Chem. Soc.* **2008**, *130*, 8608−8610.
(23) Walter, M.; Häkkinen, H. A hollow tetrahedral cage of hexadecagold dianion provides a robust backbone for a tuneable sub-nanometer oxidation and reduction agent via endohedral doping. *Phys. Chem. Chem. Phys.* **2006**, *8*, 5407−5411.
(24) Deheer, W. The physics of simple metal-clusters—Experimental aspects and simple models. *Rev. Mod. Phys.* **1993**, *65*, 611−676.
(25) Daniel, M.-C.; Astruc, D. Gold nanoparticles: Assembly, supramolecular chemistry, quantum-size-related properties, and applications toward biology, catalysis, and nanotechnology. *Chem. Rev.* **2004**, *104*, 293−346.
(26) Mathew-Fenn, R. S.; Das, R.; Harbury, P. A. B. Remeasuring the double helix. *Science* **2008**, *322*, 446−449.
(27) Crespo, P.; Litrán, R.; Rojas, T. C.; Multigner, M.; de la Fuente, J. M.; Sánchez-López, J. C.; García, M. A.; Hernando, A.; Penadés, S.; Fernández, A. Permanent magnetism, magnetic anisotropy, and hysteresis of thiol-capped gold nanoparticles. *Phys. Rev. Lett.* **2004**, *93*, No. 087204.
(28) Dass, A. Faradaurate nanomolecules: A superstable plasmonic 76.3 kDa cluster. *J. Am. Chem. Soc.* **2011**, *133*, 19259−19261.
(29) Kumara, C.; Dass, A. $(AuAg)_{144}(SR)_{60}$ alloy nanomolecules. *Nanoscale* **2011**, *3*, 3064−3067.
(30) Qian, H.; Jin, R. Controlling nanoparticles with atomic precision: The case of $Au_{144}(SCH_2CH_2Ph)_{60}$. *Nano Lett.* **2009**, *9*, 4083−4087.
(31) Qian, H.; Zhu, Y.; Jin, R. Atomically precise gold nanocrystal molecules with surface plasmon resonance. *Proc. Natl. Acad. Sci. U.S.A.* **2012**, *109*, 696−700.
(32) Knoppe, S.; Boudon, J.; Dolamic, I.; Dass, A.; Bürgi, T. Size exclusion chromatography for semipreparative scale separation of $Au_{38}(SR)_{24}$ and $Au_{40}(SR)_{24}$ and larger clusters. *Anal. Chem.* **2011**, *83*, 5056−5061.
(33) Qian, H.; Zhu, Y.; Jin, R. Isolation of ubiquitous $Au_{40}(SR)_{24}$ clusters from the 8 kDa gold clusters. *J. Am. Chem. Soc.* **2010**, *132*, 4583−4585.
(34) Kumar, S.; Jin, R. Water-soluble $Au_{25}(Capt)_{18}$ nanoclusters: Synthesis, thermal stability, and optical properties. *Nanoscale* **2012**, *4*, 4222−4227.
(35) Wu, Z.; Chen, J.; Jin, R. One-pot synthesis of $Au_{25}(SG)_{18}$ 2- and 4-nm gold nanoparticles and comparison of their size-dependent properties. *Adv. Funct. Mater.* **2010**, *21*, 177−183.
(36) Levi-Kalisman, Y.; Jadzinsky, P. D.; Kalisman, N.; Tsunoyama, H.; Tsukuda, T.; Bushnell, D. A.; Kornberg, R. D. Synthesis and characterization of $Au_{102}(p\text{-MBA})_{44}$ nanoparticles. *J. Am. Chem. Soc.* **2011**, *133*, 2976−2982.
(37) Ackerson, C. J.; Jadzinsky, P. D.; Sexton, J. Z.; Bushnell, D. A.; Kornberg, R. D. Synthesis and bioconjugation of 2 and 3 nm-diameter gold nanoparticles. *Bioconjugate Chem.* **2010**, *21*, 214−218.
(38) Negishi, Y.; Takasugi, Y.; Sato, S.; Yao, H.; Kimura, K.; Tsukuda, T. Magic-numbered Aun clusters protected by glutathione monolayers (n = 18, 21, 25, 28, 32, 39): Isolation and spectroscopic characterization. *J. Am. Chem. Soc.* **2004**, *126*, 6518−6519.
(39) Briñas, R. P.; Hu, M.; Qian, L.; Lymar, E. S.; Hainfeld, J. F. Gold nanoparticle size controlled by polymeric Au(I) thiolate precursor size. *J. Am. Chem. Soc.* **2008**, *130*, 975−982.
(40) Schaaff, T.; Whetten, R. Giant gold−glutathione cluster compounds: Intense optical activity in metal-based transitions. *J. Phys. Chem. B* **2000**, *104*, 2630−2641.
(41) Negishi, Y.; Nobusada, K.; Tsukuda, T. Glutathione-protected gold clusters revisited: Bridging the gap between gold(I)−thiolate complexes and thiolate-protected gold nanocrystals. *J. Am. Chem. Soc.* **2005**, *127*, 5261−5270.
(42) Sousa, A. A.; Morgan, J. T.; Brown, P. H.; Adams, A.; Jayasekara, M. P.; Zhang, G.; Ackerson, C. J.; Kruhlak, M. J.; Leapman, R. D. Synthesis, characterization, and direct intracellular imaging of ultrasmall and uniform glutathione-coated gold nanoparticles. *Small* **2012**, *8*, 2277−2286.
(43) Ackerson, C. J.; Jadzinsky, P. D.; Kornberg, R. D. Thiolate ligands for synthesis of water-soluble gold clusters. *J. Am. Chem. Soc.* **2005**, *127*, 6550−6551.
(44) Hainfeld, J. F.; Slatkin, D. N.; Focella, T. M.; Smilowitz, H. M. Gold nanoparticles: A new X-ray contrast agent. *Br. J. Radiol.* **2006**, *79*, 248−253.
(45) Hamad-Schifferli, K.; Schwartz, J. J.; Santos, A. T.; Zhang, S.; Jacobson, J. M. Remote electronic control of DNA hybridization through inductive coupling to an attached metal nanocrystal antenna. *Nature* **2002**, *415*, 152−5.